Contents

Chapter 1

Mathematical Formulations

1.1 Governing equations

Consider an undisturbed, steady, incompressible two-dimensional parallel flow with velocity $\vec{u} = U(z)$ and total pressure $p = P_0$. Cartesian coordinates are defined with x-axis in the streamwise direction and z-axis in the upward vertical direction. The fluid satisfies the continuity and momentum equations

$$\nabla \cdot \vec{u} = 0, \tag{1.1}$$

$$\frac{\partial \vec{u}}{\partial t} + (\vec{u} \cdot \nabla)\, \vec{u} = -\frac{1}{\rho}\nabla p + \nu \nabla^2 \vec{u}, \tag{1.2}$$

where ρ and ν are the density and kinematic viscosity of the fluid.

1.2 Boundary conditions

The flow domain is bounded on top by the free surface and extends to infinity in depth. At the upper boundary, the kinematic and dynamic boundary conditions are required to represent the presence of the free surface. The upper boundary conditions

are defined at the free surface, but since the free surface isn't a fixed boundary, the boundary conditions are set at the position of the free surface $z = \eta(x, y, t)$, where $\eta(x, y, t)$ denotes the surface elevation.

Additionally, to derive the kinematic and dynamic boundary conditions at the free surface, local coordinates are required. Given the mathematical expression of the free surface $f(x, y, t) = z - \eta(x, y, t) = 0$, its has an unit normal vector

$$\hat{n} = \frac{\nabla f}{\|\nabla f\|} = \frac{-\eta_x \hat{i} - \eta_y \hat{j} + \hat{k}}{\left(\eta_x^2 + \eta_y^2 + 1\right)^{1/2}} = (n_x, n_y, n_z), \tag{1.3}$$

where a subscript x or y of the variable η denotes a partical x- or y-derivative of η. Tangential vectors are defined to be perpendicular to the normal vector $\hat{n}$, but apart from this they are non-unique. For simplicity we define the two unit tangential vectors to be parallel to the x- and y-axes,

$$\hat{t}_x = \frac{\hat{i} + \eta_x \hat{k}}{\left(1 + \eta_x^2\right)^{1/2}}, \quad \hat{t}_x \cdot \hat{n} = 0, \tag{1.4}$$

$$\hat{t}_y = \frac{\hat{j} + \eta_y \hat{k}}{\left(1 + \eta_y^2\right)^{1/2}}, \quad \hat{t}_y \cdot \hat{n} = 0, \tag{1.5}$$

note that the two tangential vectors are not necessarily orthogonal. The local coordinate system is then formed by the unit normal and tangential vectors $(\hat{n}, \hat{t}_x, \hat{t}_y)$.

1.2.1 Kinematic boundary condition

The kinematic boundary condition states that each particle on the free surface stays on the surface, that is the material derivative of the surface remains zero,

$$\frac{Df}{Dt} = \frac{\partial f}{\partial t} + \vec{u} \cdot \nabla f = 0, \qquad \text{at } z = \eta(x, y, t), \tag{1.6}$$

With $f(x,y,t) = z - \eta(x,y,t) = 0$, the above equation can be written as

$$\begin{aligned} \frac{Df}{Dt} &= \frac{\partial}{\partial t}[z-\eta] + (\vec{u}\cdot\vec{n})\|\nabla f\| \\ &= -\frac{\partial \eta}{\partial t} - u\frac{\partial \eta}{\partial x} - v\frac{\partial \eta}{\partial y} + w = 0, \qquad \text{at } z = \eta, \end{aligned} \tag{1.7}$$

with the physical meaning that the deformation rate of the free surface equals to the flow velocity normal to the free surface.

1.2.2 Dynamic boundary condition

The dynamic boundary condition states that the stress at the free surface is balanced. One of the forces acting on the free surface is the surface tension, which exists due to the discontinuity of density at the interface of two immiscible fluids. Here the free surface act as the interface between air and water. The intermolecular forces caused the interface to be under tension, leading to a pressure jump at positions where the interface is curved. This pressure jump is related to the curvature and normal vector of the interface, its relations described by the Young-Laplace equation

$$\Delta p = -\sigma(\nabla \cdot \hat{n}) = -\sigma\kappa, \tag{1.8}$$

where σ denotes the surface tension and κ is the curvature of the free surface. In the above equation the relation $\kappa = \nabla \cdot \hat{n}$ is applied, by substituting equation (1.3), the curvature can be written as

$$\begin{aligned} \kappa &= \nabla \cdot \hat{n} \\ &= \frac{\partial n_x}{\partial x} + \frac{\partial n_y}{\partial y} + \frac{\partial n_z}{\partial z} \\ &= \frac{-\eta_{xx}\left(\eta_y^2+1\right) - \eta_{yy}\left(\eta_x^2+1\right) + 2\eta_x\eta_y\eta_{xy}}{\left(\eta_x^2+\eta_y^2+1\right)^{3/2}} \end{aligned} \tag{1.9}$$

Surface tension balances with the total stress at the free surface. The total

stress τ^s consists of stress in both air and water phases. For an incompressible, irrotational Newtonian fluid, the stress tensor is expressed as

$$\begin{aligned}\tau_{ij} &= -p\delta_{ij} + 2\mu e_{ij} \\ &= \begin{bmatrix} -p + 2\mu\frac{\partial u}{\partial x} & \mu\left(\frac{\partial v}{\partial x} + \frac{\partial u}{\partial y}\right) & \mu\left(\frac{\partial w}{\partial x} + \frac{\partial u}{\partial z}\right) \\ \mu\left(\frac{\partial v}{\partial x} + \frac{\partial u}{\partial y}\right) & -p + 2\mu\frac{\partial v}{\partial y} & \mu\left(\frac{\partial w}{\partial y} + \frac{\partial v}{\partial z}\right) \\ \mu\left(\frac{\partial w}{\partial x} + \frac{\partial u}{\partial z}\right) & \mu\left(\frac{\partial w}{\partial y} + \frac{\partial v}{\partial z}\right) & -p + 2\mu\frac{\partial w}{\partial z} \end{bmatrix},\end{aligned} \tag{1.10}$$

where p is the total pressure. Therefore total stress acting on the free surface are derived by applying the stress tensor

$$\begin{aligned}[\tau]\cdot\{\hat{n}\}^T &= \tau_{ij}n_j \\ &= \frac{\mu}{\left(\eta_x^2+\eta_y^2+1\right)^{1/2}}\left\{\left[\eta_x\frac{p}{\mu} - 2\eta_x\frac{\partial u}{\partial x} - \eta_y\left(\frac{\partial v}{\partial x}+\frac{\partial u}{\partial y}\right) + \left(\frac{\partial w}{\partial x}+\frac{\partial u}{\partial z}\right)\right]\hat{i}\right. \\ &\quad + \left[\eta_y\frac{p}{\mu} - 2\eta_y\frac{\partial v}{\partial y} - \eta_x\left(\frac{\partial v}{\partial x}+\frac{\partial u}{\partial y}\right) + \left(\frac{\partial w}{\partial y}+\frac{\partial v}{\partial z}\right)\right]\hat{j} \\ &\quad \left. + \left[-\frac{p}{\mu} + 2\frac{\partial w}{\partial z} - \eta_x\left(\frac{\partial w}{\partial x}+\frac{\partial u}{\partial z}\right) - \eta_y\left(\frac{\partial w}{\partial y}+\frac{\partial v}{\partial z}\right)\right]\hat{k}\right\}.\end{aligned} \tag{1.11}$$

To satisfy the dynamic boundary condition, the total stress must be balanced with surface tension,

$$[\tau]\cdot\{\hat{n}\}^T = -\sigma\kappa\hat{n}. \tag{1.12}$$

To further simplify the boundary condition, we apply the above equation in three directions. Since the surface tension only has effect in the direction of the normal vector of the free surface, the stress balance is inspected in the normal and tangential directions of the free surface. Therefore, in the normal direction the $\hat{n}$ component of the total stress are balanced by the surface tension, while in the tangential directions

the total stress sums up to zero

$$\{\hat{n}\}\cdot[\tau]\cdot\{\hat{n}\}^T = -\sigma\kappa, \tag{1.13}$$

$$\{\hat{t_x}\}\cdot[\tau]\cdot\{\hat{n}\}^T = 0, \tag{1.14}$$

$$\{\hat{t_y}\}\cdot[\tau]\cdot\{\hat{n}\}^T = 0. \tag{1.15}$$

Substitute equations (1.9) and (1.11) into the above equations,

$$\begin{aligned} -p + \frac{2\mu}{\eta_x^2+\eta_y^2+1}\left[\eta_x^2\frac{\partial u}{\partial x} + \eta_y^2\frac{\partial v}{\partial y} + \frac{\partial w}{\partial z} + \eta_x\eta_y\left(\frac{\partial v}{\partial x}+\frac{\partial u}{\partial y}\right) - \eta_x\left(\frac{\partial w}{\partial x}+\frac{\partial u}{\partial z}\right)\right. \\ \left. -\eta_y\left(\frac{\partial w}{\partial y}+\frac{\partial v}{\partial z}\right)\right] = \sigma\frac{\eta_{xx}\left(\eta_y^2+1\right)+\eta_{yy}\left(\eta_x^2+1\right)-2\eta_x\eta_y\eta_{xy}}{\left(\eta_x^2+\eta_y^2+1\right)^{3/2}}, \end{aligned} \tag{1.16}$$

$$\begin{aligned} 2\eta_x\left(\frac{\partial w}{\partial z}-\frac{\partial u}{\partial x}\right) - \eta_y\left(\frac{\partial u}{\partial y}+\frac{\partial v}{\partial x}\right) + \left(1-\eta_x^2\right)\left(\frac{\partial w}{\partial x}+\frac{\partial u}{\partial z}\right) \\ -\eta_x\eta_y\left(\frac{\partial v}{\partial z}+\frac{\partial w}{\partial y}\right) = 0, \end{aligned} \tag{1.17}$$

$$\begin{aligned} 2\eta_y\left(\frac{\partial w}{\partial z}-\frac{\partial v}{\partial y}\right) - \eta_x\left(\frac{\partial u}{\partial y}+\frac{\partial v}{\partial x}\right) + \left(1-\eta_y^2\right)\left(\frac{\partial w}{\partial y}+\frac{\partial v}{\partial z}\right) \\ -\eta_x\eta_y\left(\frac{\partial u}{\partial z}+\frac{\partial w}{\partial x}\right) = 0. \end{aligned} \tag{1.18}$$

1.2.3 Boundary condition at infinity

The flow domain extends to infinity in depth, and the boundary conditions is that the disturbance vanishes at infinite depth,

$$u', w' \to 0, \text{ as } z \to -\infty. \tag{1.19}$$

Chapter 2

Linear Stability Analysis of Flow

2.1 Stability analysis

2.1.1 Temporal and spatial stability

The temporal stability analysis is performed by constraining the wavenumber k to be a real number, in other words, the amplitude of the perturbation waves neither grow nor decay with space. For a fixed real wavenumber ($k \in \mathbb{R}$), the associated complex frequencies ($\omega \in \mathbb{C}$) are found by solving the dispersion relation (2.14). The imaginary part of ω is known as the growth rate of the perturbation (ω_i) so that the flow grows with time for a positive value, while decays with time for a negative value. The stability of the flow is then dominated by the most unstable mode, which is the mode with the largest growth rate $\omega_{i,max}$.

The concept of spatial stability analysis is similar to the temporal approach, where real frequencies ($\omega \in \mathbb{R}$) are considered, and the dispersion relation gives complex wavenumbers ($k \in \mathbb{C}$). The imaginary part of the wavenumber decides whether the perturbation grows or decays within space.

2.1.2 Spatial-temporal stability

2.2 Orr-Sommerfeld equation

Linear stability analysis of the flow is investigated by introducing two-dimensional perturbations into the flow, which grow or decay with time. The perturbed flow has velocity $\vec{u} = U(z) + \vec{u'}(x, z, t)$, and pressure $p = P_0 + p'(x, z, t)$, where the order of the perturbations $\mathcal{O}(\vec{u'}/U), \mathcal{O}(p'/P_0) \ll 1$. By substituting the perturbed velocity and pressure into equation (1.1) and (1.2), the continuity and momentum equations became

$$\frac{\partial u'}{\partial x} + \frac{\partial w'}{\partial z} = 0, \tag{2.1}$$

$$\frac{\partial u'}{\partial t} + (U + u')\frac{\partial (U + u')}{\partial x} + w'\frac{d(U + u')}{dz} = -\frac{1}{\rho}\frac{\partial (P_0 + p')}{\partial x} + \nu\left(\frac{\partial^2 (U + u')}{\partial x^2} + \frac{\partial^2 (U + u')}{\partial z^2}\right), \tag{2.2}$$

$$\frac{\partial w'}{\partial t} + (U + u')\frac{\partial w'}{\partial x} = -\frac{1}{\rho}\frac{\partial (P_0 + p')}{\partial z} + \nu\left(\frac{\partial^2 w'}{\partial x^2} + \frac{\partial^2 w'}{\partial z^2}\right). \tag{2.3}$$

Neglecting the high order terms in equations (2.1), (2.2), and (2.3),

$$\frac{\partial u'}{\partial x} + \frac{\partial w'}{\partial z} = 0, \tag{2.4}$$

$$\frac{\partial u'}{\partial t} + U\frac{\partial u'}{\partial x} + w'\frac{dU}{dz} = -\frac{1}{\rho}\frac{\partial p'}{\partial x} + \nu\left(\frac{\partial^2 u'}{\partial x^2} + \frac{\partial^2 u'}{\partial z^2}\right), \tag{2.5}$$

$$\frac{\partial w'}{\partial t} + U\frac{\partial w'}{\partial x} = -\frac{1}{\rho}\frac{\partial p'}{\partial z} + \nu\left(\frac{\partial^2 w'}{\partial x^2} + \frac{\partial^2 w'}{\partial z^2}\right). \tag{2.6}$$

By differentiating equation (2.5) with z and equation (2.6) with x, the two equations can be combined, with the pressure terms eliminated

$$\frac{\partial}{\partial z}\left[\frac{\partial u'}{\partial t} + U\frac{\partial u'}{\partial x} + w'\frac{dU}{dz} - \nu\left(\frac{\partial^2 u'}{\partial x^2} + \frac{\partial^2 u'}{\partial z^2}\right)\right] - \frac{\partial}{\partial x}\left[\frac{\partial w'}{\partial t} + U\frac{\partial w'}{\partial x} - \nu\left(\frac{\partial^2 w'}{\partial x^2} + \frac{\partial^2 w'}{\partial z^2}\right)\right] = 0. \tag{2.7}$$

The two governing equations (2.4) and (2.7) may be reduced into one by intro-

ducing a perturbation stream function $\psi(x, z, t)$ defined as

$$u'(x, z, t) = \frac{\partial \psi(x, z, t)}{\partial z}, \quad w'(x, z, t) = -\frac{\partial \psi(x, y, t)}{\partial x}, \tag{2.8}$$

which satisfies the continuity equation (2.4). In terms of the stream function, equation (2.7) became

$$\left(\frac{\partial}{\partial t} + U\frac{\partial}{\partial x}\right)\left(\frac{\partial^2 \psi}{\partial z^2} + \frac{\partial^2 \psi}{\partial x^2}\right) - \frac{d^2 U}{dz^2}\frac{\partial \psi}{\partial x} - \nu\left(\frac{\partial^4 \psi}{\partial x^4} + \frac{\partial^4 \psi}{\partial z^4} + 2\frac{\partial^4 \psi}{\partial x^2 \partial z^2}\right) = 0. \tag{2.9}$$

The perturbation is arbitrary in form, so we may seek normal mode solutions to the problem. By a normal mode expansion in the streamwise direction, the stream function has the form

$$\psi(x, z, t) = \int_0^\infty \phi(z) e^{ik(x-ct)}\, dk, \tag{2.10}$$

where k is the streamwise wavenumber, and c represents the phase velocity. Upon substituting the above expression into equation (2.9), which is equivalent to doing a Fourier transform in the streamwise direction, we obtain a fourth-order ordinary differential equation

$$kU\left(\phi_{zz} - k^2\phi\right) + kU_{zz}\phi - i\nu\left(\phi_{zzzz} - k^2\phi_{zz} + k^4\phi\right) = \omega\left(\phi_{zz} - k^2\phi\right), \tag{2.11}$$

where $\omega = kc$ is the frequency, and a subscript z denotes a z-derivative. This equation is known as the Orr-Sommerfeld equation, which governs the stability of locally parallel flows. A dimensionless form of the equation, with the free-flow velocity U_∞ as characteristic velocity $[\mathcal{V}]$ and the half-width of the wake b as characteristic length $[\mathcal{L}]$, gives

$$\tilde{k}\tilde{U}\left(\tilde{\phi}_{zz} - \tilde{k}^2\tilde{\phi}\right) + \tilde{k}\tilde{U}_{zz}\tilde{\phi} - \frac{i}{Re}\left(\tilde{\phi}_{zzzz} - \tilde{k}^2\tilde{\phi}_{zz} + \tilde{k}^4\tilde{\phi}\right) = \tilde{\omega}\left(\tilde{\phi}_{zz} - \tilde{k}^2\tilde{\phi}\right), \tag{2.12}$$

where a tilde (˜) represents a dimensionless variable. The Reynolds number is defined as $Re = [\mathcal{V}][\mathcal{L}]/\nu$, representing the ratio of the inertia force to the viscous force in a fluid. In cases that viscous forces are negligible, the governing equation can be derived by letting $Re \to \infty$ in the dimensionless Orr-Sommerfeld equation (2.12), giving

$$\tilde{k}\tilde{U}\tilde{\phi}_{zz} - \tilde{k}^3\tilde{U}\tilde{\phi} + \tilde{k}\tilde{U}_{zz}\tilde{\phi} = \tilde{\omega}\left(\tilde{\phi}_{zz} - \tilde{k}^2\tilde{\phi}\right), \tag{2.13}$$

which is known as the Rayleigh equation. Dimensionless forms of the governing equations are used throughout the thesis, for simplicity the tilde (˜) expressions are dropped, and the variables are by default dimensionless if not specified otherwise.

Associated with appropriate boundary conditions, the Orr-Sommerfeld equation and the Rayleigh equation may be solved. Non-trivial solutions can be found only if the variables k and ω satisfy the dispersion relation

$$D(k, \omega; Re) = 0. \tag{2.14}$$

The wavenumber k and frequency ω are generally complex variables but may be altered when considering specific stability problems. In the following sections, this dispersion relation is used extensively in temporal, spatial, and spatial-temporal stability problems.

2.3 Boundary conditions

In this section the boundary conditions for linear stability analysis are derived by adapting the equations in Chapter 1.2. The flow is assumed to be two-dimensional, with disturbance added and expanded in normal modes.

2.3.1 Kinematic boundary condition

Two dimensional, dimensionless expression of the kinematic boundary condition (1.7) at the free surface, with perturbations included,

$$\frac{\partial \eta}{\partial t} + (U + u')\frac{\partial \eta}{\partial x} - w' = 0, \qquad \text{at } z = \eta. \tag{2.15}$$

For simplicity in numerical computations, the boundary conditions are expected to be defined at fixed locations, hence we expand the above equation with Taylor series at $z = 0$,

$$\frac{\partial \eta}{\partial t} + \left[U + u' + \eta\frac{\partial U}{\partial z} + \eta\frac{\partial u'}{\partial z} + \mathcal{O}(\eta^2)\right]\frac{\partial \eta}{\partial x} - \left[w' + \eta\frac{\partial w'}{\partial z} + \mathcal{O}(\eta^2)\right] = 0. \tag{2.16}$$

Assume perturbed velocity and surface elevation are small quantities $|u'|, |w'|, |\eta| \ll 1$, and products of the small quantities are neglected, resulting in

$$\frac{\partial \eta}{\partial t} + U\frac{\partial \eta}{\partial x} - w = 0, \qquad \text{at } z = 0. \tag{2.17}$$

By applying normal mode expansion to the perturbed velocity and surface elevation,

$$kUq + k\phi = \omega q, \qquad \text{at } z = 0, \tag{2.18}$$

where $\eta(x, t) = qe^{i(kx-\omega t)}$.

2.3.2 Dynamic boundary condition

$$\frac{2\eta_x}{Re}\left(\frac{\partial w}{\partial z} - \frac{\partial u}{\partial x}\right) + \frac{(1-\eta_x^2)}{Re}\left(\frac{\partial u}{\partial z} + \frac{\partial w}{\partial x}\right) = 0. \tag{2.19}$$

$$-p + \frac{\eta}{Fr^2} + \frac{1}{Re}\frac{2}{(\eta_x^2+1)}\left[\eta_x^2\frac{\partial u}{\partial x} + \frac{\partial w}{\partial z} - \eta_x\left(\frac{\partial u}{\partial z}\right)\right] = \frac{1}{We}\frac{\eta_{xx}}{(\eta_x^2+1)^{3/2}}. \tag{2.20}$$

$$\frac{2\eta_x}{Re}\left(\frac{\partial w}{\partial z}-\frac{\partial u}{\partial x}\right)+\frac{(1-\eta_x^2)}{Re}\left(\frac{\partial u}{\partial z}+\frac{\partial w}{\partial x}\right)=0. \tag{2.21}$$

$$-p+\frac{\eta}{Fr^2}+\frac{1}{Re}\frac{2}{(\eta_x^2+1)}\left[\eta_x^2\frac{\partial u}{\partial x}+\frac{\partial w}{\partial z}-\eta_x\left(\frac{\partial u}{\partial z}\right)\right]=0, \tag{2.22}$$

The dynamic boundary condition states that the total stress at the free surface is balanced. Detailed stress balance relations are derived in Appendix 4.1. The effect of surface tension and disturbance in the air is neglected, and the normal and tangential stress balance equations (**??**) and (**??**) are

$$\frac{2\eta_x}{Re}\left(\frac{\partial w}{\partial z}-\frac{\partial u}{\partial x}\right)+\frac{(1-\eta_x^2)}{Re}\left(\frac{\partial u}{\partial z}+\frac{\partial w}{\partial x}\right)=0. \tag{2.23}$$

$$-p+\frac{\eta}{Fr^2}+\frac{1}{Re}\frac{2}{(\eta_x^2+1)}\left[\eta_x^2\frac{\partial u}{\partial x}+\frac{\partial w}{\partial z}-\eta_x\left(\frac{\partial u}{\partial z}\right)\right]=0. \tag{2.24}$$

First consider the tangential stress condition equation (2.23). By replacing the velocities by the sum of background flow and perturbation flow velocities,

$$\frac{2\eta_x}{Re}\left(\frac{\partial w'}{\partial z}-\frac{\partial u'}{\partial x}\right)+\frac{(1-\eta_x^2)}{Re}\left(\frac{\partial U}{\partial z}+\frac{\partial u'}{\partial z}+\frac{\partial w'}{\partial x}\right)=0. \tag{2.25}$$

The above equation is defined at $z=\eta$, so again we expand the equation at $z=0$ with Taylor series expansion and neglect high order terms, equation (2.25) is reduced to

$$\eta\frac{\partial^2 U}{\partial z^2}+\frac{\partial u'}{\partial z}+\frac{\partial w'}{\partial x}=0, \tag{2.26}$$

with the fact that $(\partial U/\partial z)|_{z=0}=0$. Normal mode expansion of the above equation yields the tangential stress condition,

$$qU_{zz}+\phi_{zz}+k^2\phi=0. \tag{2.27}$$

Next the normal stress condition with disturbance is derived. By implementing perturbation forms into equation (2.24), then apply Taylor series expansion at $z=0$

with high order terms neglected, the equation is reduced to

$$-p' + \frac{\eta}{Fr^2} + \frac{2}{Re}\frac{\partial w'}{\partial z} = 0. \tag{2.28}$$

The pressure term can be replaced using the dimensionless form of the x-direction momentum equation (2.5) and by differentiating equation (2.28) with x,

$$\frac{\partial u'}{\partial t} + U\frac{\partial u'}{\partial x} + w'\frac{dU}{dz} - \frac{1}{Re}\left(\frac{\partial^2 u'}{\partial x^2} + \frac{\partial^2 u'}{\partial z^2}\right) + \frac{\eta_x}{Fr^2} + \frac{2}{Re}\frac{\partial^2 w'}{\partial x \partial z} = 0. \tag{2.29}$$

Normal mode expansion of the above equation yields the normal stress condition,

$$kU\phi_z - k\phi\frac{dU}{dz} + \frac{i}{Re}\left(\phi_{zzz} - 3k^2\phi_z\right) + \frac{k}{Fr^2}q = \omega\phi_z. \tag{2.30}$$

2.3.3 Boundary condition at infinity

$$\phi, \phi_z \to 0, \text{ as } z \to -\infty. \tag{2.31}$$

Chapter 3

Numerical Methods

3.1 Chebyshev collocation method

Linear stability analysis is performed by solving the governing equations, the Orr-Sommerfeld equation (2.12) when considering viscosity effects, and the Rayleigh equation (2.13) for inviscid assumptions, along with the boundary conditions. The spectral collocation method with Chebyshev polynomials is used to discretize the eigenvalue problem in the vertical direction.

The concept of the spectral methods implies that unknown functions in the governing equations are expanded using a series expansion, which we chose Chebyshev polynomials of the first kind as the basis functions. Chebyshev polynomials are defined on the interval $\zeta \in [-1, 1]$, and the n-th Chebyshev polynomial is defined as

$$T_n(\zeta) = \cos(n \cos^{-1}(\zeta)). \tag{3.1}$$

The unknown functions shall be represented with the Chebyshev polynomials. To implement the Chebyshev polynomial, the physical domain $z \in [-h, 0]$ is mapped

to the computational domain $\zeta \in [-1, 1]$ via coordinate transform

$$\zeta = \frac{2z}{h} + 1, \quad -h \leq z \leq 0. \tag{3.2}$$

In the computational domain, the eigenfunction ϕ is expanded using the Chebyshev expansion

$$\phi(\zeta) = \sum_{n=0}^{N} a_n T_n(\zeta), \tag{3.3}$$

where N represents the N-th Chebyshev polynomial and a_n is the coefficient of the series. Coefficient a_n's replace $\phi(\zeta)$'s as unknown variables to be solved, with the difference that a_n's are independent of ζ. The derivatives of $\phi(\zeta)$ in the vertical direction are also represented in expanded form, by using chain-rule,

$$\frac{d^j \phi(\zeta)}{dz^{(j)}} = \left(\frac{2}{h}\right)^j \sum_{n=0}^{N} a_n T_n^{(j)}(\zeta). \tag{3.4}$$

Here the (j)-th order derivative with respect to ζ of the Chebyshev polynomial $T_n^{(j)}(\zeta)$ is involved, and an advantage of the Chebyshev polynomial is that its derivatives can be derived recursively using lower order terms. As stated in Schmid & Henningson (2001) [4],

$$\begin{aligned} &T_0^{(j)}(\zeta) = 0, \quad T_1^{(j)}(\zeta) = T_0^{(j-1)}(\zeta), \quad T_2^{(j)}(\zeta) = 4T_1^{(j-1)}(\zeta), \\ &T_{n+1}^{(j)}(\zeta) = 2(n+1)T_n^{(j-1)}(\zeta) + \frac{n+1}{n-1} T_{n-1}^{(j)}(\zeta) \quad n \geq 2. \end{aligned} \tag{3.5}$$

By applying the above relations, the derivatives of $\phi(\zeta)$ can be replaced by linear combinations of $T_n(\zeta)$, so that the problem is now a linear algebraic system.

The system is discretized with the use of the collocation method. We evaluate the Chebyshev polynomials at chosen locations, with the restriction that the governing equations be satisfied at these discrete collocation points $(\zeta_1, \zeta_2, ..., \zeta_{M-1})$, defined as

$$\zeta_m = \cos(\frac{\pi m}{M}), m = 1, 2, ..., M-1. \tag{3.6}$$

This distribution of points is known as the Gauss-Lobatto points and is chosen to minimize the effect of Runge's phenomenon.

Instead of applying governing equations to the boundaries, we replace them with the boundary conditions derived in previous sections. Considering viscosity, free surface conditions (2.18), (2.27), and (2.30) are applied at the upper boundary $\zeta = \zeta_0 = 1$, while free-slip conditions (3.8) are applied at the lower boundary $\zeta = \zeta_M = -1$. This results in a total of $M + 4$ equations determining $N + 2$ unknowns, with $N + 1$ coefficients of the $N + 1$ Chebyshev polynomials and the amplitude of surface elevation q. For the system to be exactly determined, we choose $M = N - 2$.

For inviscid assumptions, the tangential stress condition (2.27) is excluded at the free surface, and the exponential decaying condition (3.11) is applied at the lower boundary. With a total of $M + 2$ equations and $N + 2$ unknown, we can simply set $M = N$, so that the number of collocation points equals the order of Chebyshev polynomial used.

The ODE system is then rearranged into a linear algebraic generalized eigenvalue problem (GEP), in mathematical form $\boldsymbol{A}\boldsymbol{x} = \omega\boldsymbol{B}\boldsymbol{x}$, with eigenvalue $\omega = kc$ and eigenvector $\boldsymbol{x}^T = [a_0, a_1, ..., a_N, q]$.

3.2 Treatment on infinity boundary

To perform numerical computation, the infinite boundary is treated by truncating the domain to a finite truncation height h, and we derive two different methods of the boundary condition (1.19) at the truncation height. The two treatments are compared in chapter (4).

The first treatment is done by replacing the boundary condition (1.19) by the

free-slip condition

$$\left.\frac{\partial u}{\partial z}\right|_{z=-h} = w|_{z=-h} = 0, \tag{3.7}$$

with the fact that $dU/dz = 0$ and normal mode expansion,

$$\frac{d^2\phi(-h)}{dz^2} = \phi(-h) = 0. \tag{3.8}$$

Another treatment is that by implementing the condition that at infinity depth, the velocity of the background flow approaches the free-stream velocity $U = 1$, and thus $d^2U/dz^2 = 0$. Asymptotic solutions of the governing equation (2.12) can be solved analytically, approaching four independent exponential solutions

$$\phi(z) = C_1 e^{kz} + C_2 e^{-kz} + C_3 e^{\left(\sqrt{k^2+ikRe}\right)z} + C_4 e^{-\left(\sqrt{k^2+ikRe}\right)z}. \tag{3.9}$$

The boundary condition (1.19) states that perturbation velocity vanishes at infinity, thus only decaying solutions in equation (3.9) remains. Considering only the dominant terms, the solution is simplified into $\phi(z) = C_1 \exp(kz)$. Therefore at a sufficiently low truncation height $z = -h$, the stream function amplitude became

$$\phi(-h) = C_1 e^{-kh}, \tag{3.10}$$

which is the modified boundary condition. To apply this boundary condition to system with the Orr-Sommerfeld equation (2.12) as governing equation, two boundary condition equations are needed. It is done by deriving the z-derivatives of the stream function amplitude

$$\begin{aligned} \phi_z(-h) &= kC_1 e^{-kh} &&= k\phi\left(-h\right) \\ \phi_{zz}(-h) &= k^2 C_1 e^{-kh} &&= k^2\phi\left(-h\right), \end{aligned} \tag{3.11}$$

so that the exponential solution is applied and satisfied without solving for the constant C_1. Under inviscid assumptions, the boundary condition is simply represented

by the relation with its first derivative $\phi_z(-h) = k\phi(-h)$.

3.3 Generalized eigenvalue problem

Multiple methods can be considered for solving the GEPs, basically done by implementing the MATLAB built-in function `eig`, which by default uses the QZ algorithm to solve the GEPs. A GEP can be converted into a standard eigenvalue problem of the form $\boldsymbol{C}\boldsymbol{x} = \lambda\boldsymbol{x}$ by inverting either matrix $\boldsymbol{A}$ or $\boldsymbol{B}$, with the premise that the matrices are invertible. However, our boundary conditions and matching conditions without ω terms generate rows of zeros in the matrix $\boldsymbol{B}$, which causes matrix $\boldsymbol{B}$ to be singular and thus not invertible. Two different methods are used to solve this type of GEP, their convergence of eigenvalue with the increase of matrix size are compared subsequently.

The first method is the QZ algorithm mentioned above. The QZ algorithm was designed by Moler & Stewart (1973) [3] to solve problems with a singular or nearly singular matrix $\boldsymbol{B}$, and no inversions of the matrix $\boldsymbol{B}$ are used when solving for the eigenvalue. While with the advantage of solving most GEPs regardless of the singularity of matrices, the computational time for the QZ algorithm increases significantly with the increase of matrix size.

The second method was mentioned in Schmid & Henningson (2001) in [4], which the main concept of the method is to make matrix $\boldsymbol{B}$ non-singular, for the GEP to be converted to and solved as a standard eigenvalue problem. It is done by replacing the rows of zeros in matrix $\boldsymbol{B}$ by a complex multiple of its corresponding matrix $\boldsymbol{A}$. This operation doesn't affect the solutions of the original equations but produces additional artificial eigenvalues which originally are undefined. These artificial eigenvalues can easily be located and excluded since they are mapped to a specific location in the complex plane by the chosen complex multiple. With both matrices non-singular, the GEP can be converted into a standard eigenvalue

problem, either $(\boldsymbol{B}^{-1}\boldsymbol{A})\boldsymbol{x} = \omega\boldsymbol{x}$ or $(\boldsymbol{A}^{-1}\boldsymbol{B})\boldsymbol{x} = (1/\omega)\boldsymbol{x}$.

balancing

3.4 Domain decomposition method

The distribution of collocation points is fixed to the Gauss-Lobatto points, which are dense near the boundaries and sparse in between. This is sufficient for most problems, where flow properties vary most abruptly near the boundaries that require more collocation points to resolve the variations. Nevertheless, there are still cases that rapid changes of flow properties occur far from the boundaries, hence accentuating the defect in the collocation method.

In our problem, this issue arises in inviscid cases where the Rayleigh equation (2.13) has a regular singular point at a point z_0 with $U(z_0) = c$. The corresponding real part of this point defines the critical point z_c where $U(z_c) = c_r$. For cases with a small imaginary part of the phase velocity, the singularity locates near the real axis, causing abrupt variations of the eigenfunction near the critical point. To resolve the eigenfunction, dense collocation points are required in the neighborhood around the critical point, which doesn't match the collocation point distribution for critical points far from the boundaries. Consequently, a method that preserves the property of the Gauss-Lobatto points while improving the flexibility of the collocation point method is required.

We introduce the domain decomposition method, which is aimed at resolving the rapid variations of the eigenfunction. This is done by splitting the computational domain into multiple smaller domains, with a set of Gauss-Lobatto points in each domain. The distribution of collocation points is then dense near each boundary of smaller domains, therefore by splitting the computational domain at a specific location the density of distribution of points around it is increased. The bound-

aries between domains are defined by sufficient matching conditions, for inviscid problem the matching condition denotes the continuity of eigenfunction and its first derivative,

$$\phi_{(k),-} = \phi_{(k+1),+}, \quad \frac{d\phi_{(k),-}}{dz} = \frac{d\phi_{(k+1),+}}{dz}, \tag{3.12}$$

where (k) is the the split domain number, in increasing order with decreasing depth. The minus sign denotes the lower boundary and the plus sign denotes the upper boundary of each domain. With viscosity considered, a total of four equations are required at each split point, thus the matching condition is the continuity of eigenfunction up to third order,

$$\phi_{(k),-} = \phi_{(k+1),+}, \ \frac{d\phi_{(k),-}}{dz} = \frac{d\phi_{(k+1),+}}{dz}, \ \frac{d^2\phi_{(k),-}}{dz^2} = \frac{d^2\phi_{(k+1),+}}{dz^2}, \ \frac{d^3\phi_{(k),-}}{dz^3} = \frac{d^3\phi_{(k+1),+}}{dz^3}. \tag{3.13}$$

As shown above, the number of matching conditions is chosen flexibly to match the total equation needed to exactly determine the system.

The domain decomposition method improves the accuracy of problems by splitting the computational domain at locations with abrupt eigenfunction variations so that the distribution of collocation points is modified while preserving the advantage of using Gauss-Lobatto points. By applying this method to our inviscid problem, the computational domain is split at the critical height z_c, resulting in two smaller domains. For extreme cases that the critical point is nearly singular, the variation of eigenfunction became steeper and more difficult to be resolved around the critical point. Consequently, the domain is further split slightly above and below z_c to increase resolutions, resulting in four domains with two in the small neighborhood around the critical point. The number of collocation points allocated to each domain is decided by the size and convergence of the domain, which will be discussed in section 3.5.

Ideally, the computational domain is split at the critical point, but its location is initially unknown. The goal is to find the most accurate result with enough

resolution near the critical point, so a guessed location of critical point is given initially, and if the resolution of this distribution of points is enough to compute for an eigenvalue, a critical point can be calculated with this eigenvalue. This calculated critical point is then applied to split the domain to compute for a more accurate eigenvalue and critical point. The iteration continues until the computed eigenvalue converges up to an acceptable precision, in our case a magnitude difference beneath 10^{-8} with its previous iteration is considered sufficient.

The initial guess of the location of the critical point highly affects cases with singularity near the real axis, in which a wrong choice of initial split point may lead to too low a resolution to even find an inaccurate eigenvalue. However, for most cases, the choice of initial split point doesn't affect the result but only the converging rate of the eigenvalue. Therefore we choose the inflection point of the background flow velocity profile as the initial split point, which is a known parameter, and single-domain results show that it may relate to the location of critical points. For cases that fail to find an eigenvalue with this initial guess, its initial split location is set as the critical point of a successful case with similar input parameters. For instance, after failing to find an eigenvalue at a high wavenumber, we compute the critical point at a lower wavenumber, then gradually increase the wavenumber and implement the known critical point as its initial split location. Eventually, an adequate initial split location for the target wavenumber can be adapted.

3.5 Convergence test on numerical methods

Several numerical methods mentioned in this chapter are tested and compared in this section, and a specific combination of methods will be chosen as the standard numerical method for solving our wake problem. The test case is set with $Fr = 1.5$, $k = 1.5$, and $Re = 1000$ if viscosity is considered. By calculating the difference between the maximum growth rates of the test cases and the most accurate result,

the convergence can be examined and compared. Methods are then chosen based on its convergence rate and computational time.

3.5.1 Treatment on infinity boundary

To compare the two different treatments of the truncated infinity boundary, we compare the convergence of the growth rate with truncation height h for both methods. Expecting that for different wavelength the perturbation affects the background flow up to different depths, we assume that the truncation height varies with the wavelength of the perturbation. With larger truncation heights, the boundary conditions approaches the conditions at infinity, and the results are considered more accurate. Therefore the error of each case is expressed as the difference between its growth rate and the most accurate result $\omega_{0,i}$, which is computed using the largest truncation height, $h_0 = 5\lambda$ in our computation.

Consider viscous problem with $Re = 1000$, the convergence of applying free-slip condition and exponential decay are shown in Figure 3.1. The difference between the two methods is significant, as the results using exponential decay converge much faster then using the free-slip condition. From Figure 3.1(a) all the results using free-slip condition converge to 10^{-12} with the truncation height around 3λ, while from Figure 3.1(b) all the results converge to 10^{-12} at around 2λ when applying the exponential decay condition. As a conservative estimate, we choose the exponential decay treatment at the lower boundary with truncation height $h = 3\lambda$.

Similar results are shown for inviscid problems, as presented in Figure 3.2

3.5.2 Domain decomposition method

As described in section 3.4, the domain may be split into two at the critical height, or further more split into four with two additional domains split slightly

above and below the critical height. In this section the difference between the above two domain decomposition methods is analyzed, and compared with the results using the original collocation point distribution.

3.5.3 Comparison of GEP solving algorithms

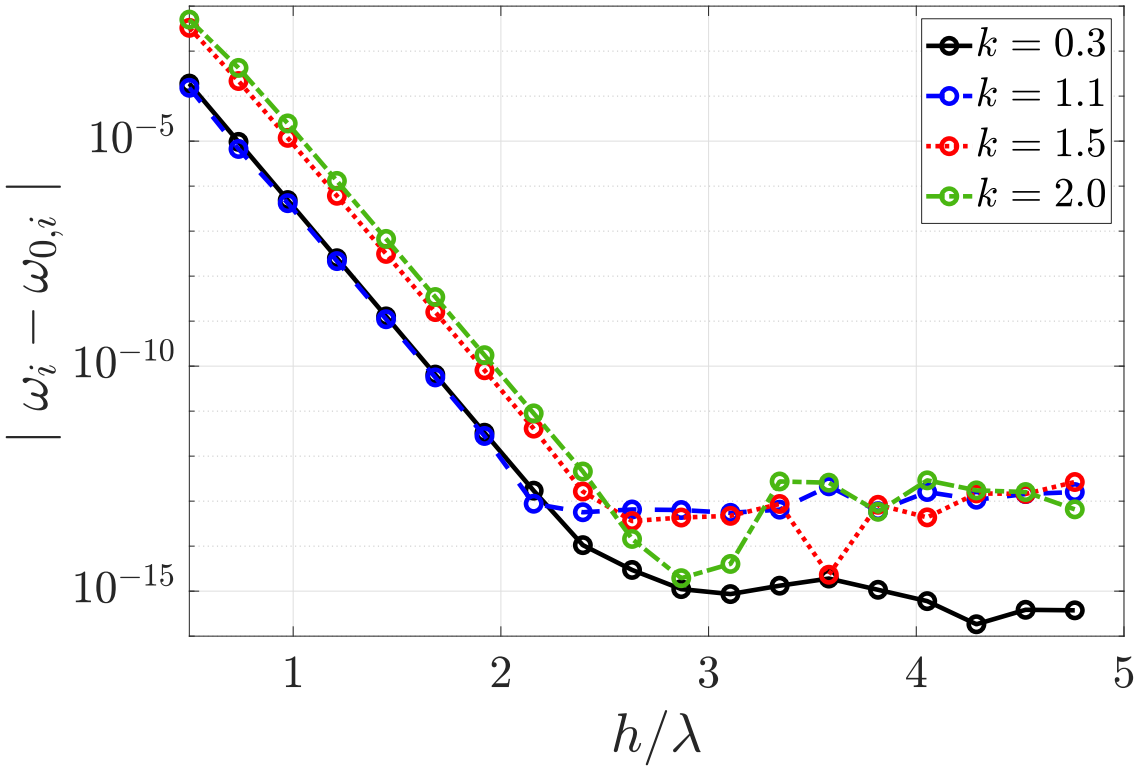

(a)

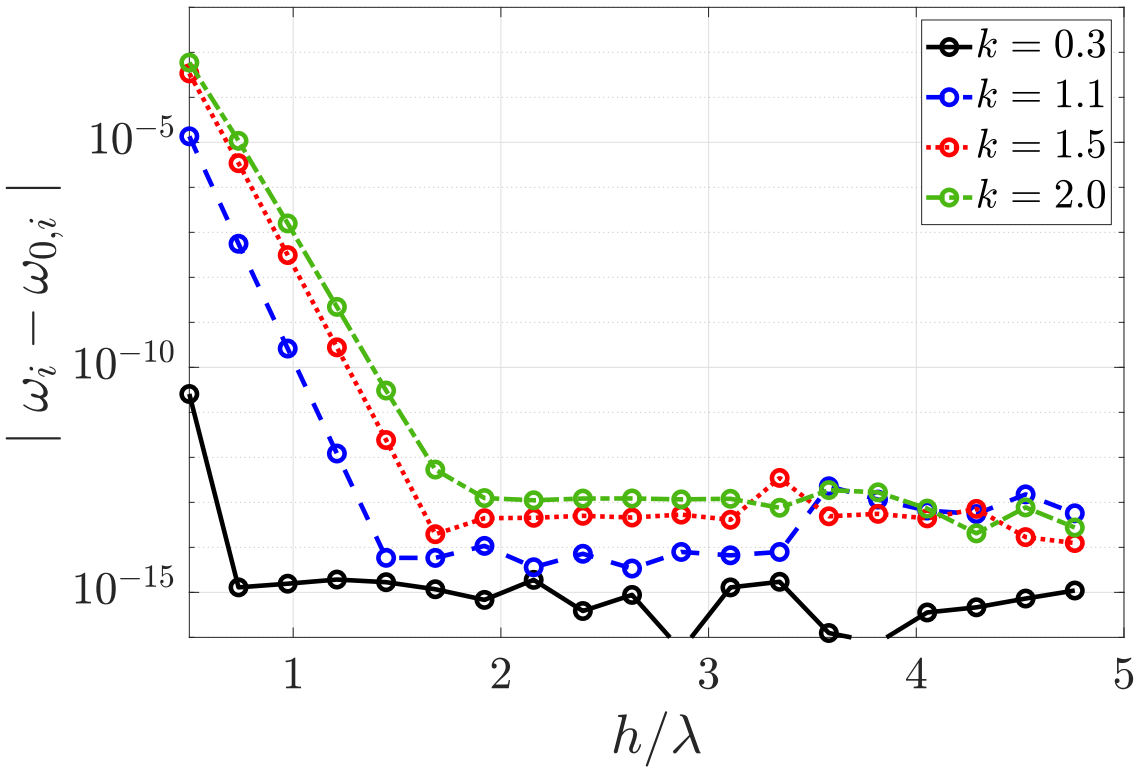

(b)

Figure 3.1: Convergence of truncation height at $Re = 1000$. (a) Free-slip condition, (b) Exponential decay.

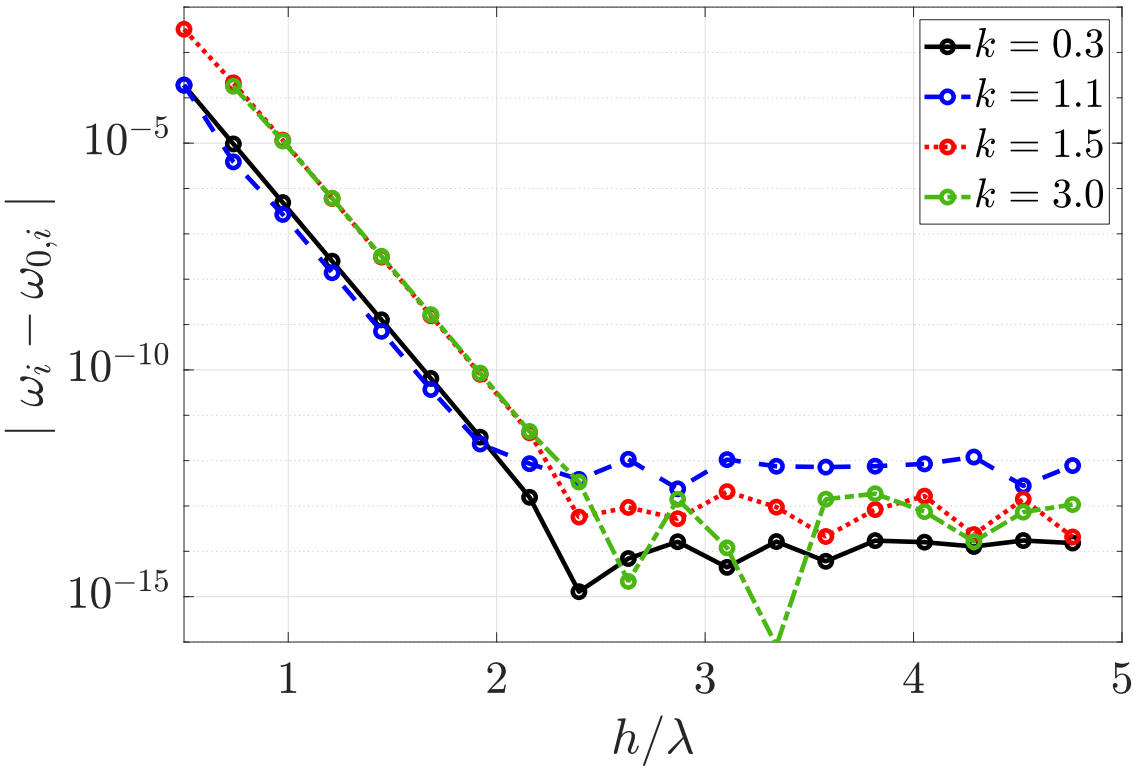

(a)

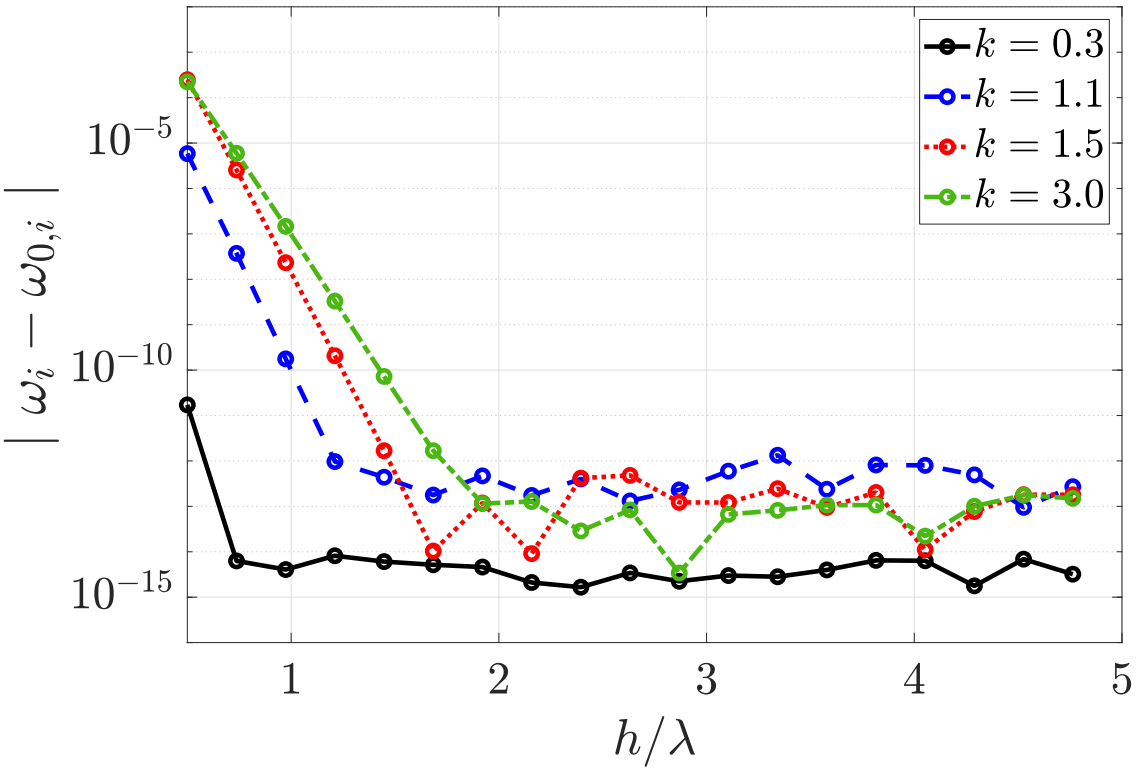

(b)

Figure 3.2: Convergence of truncation height at $Re = \infty$. (a) Free-slip condition, (b) Exponential decay.

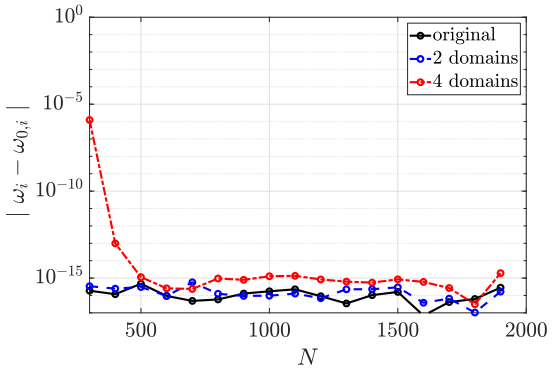

(a)

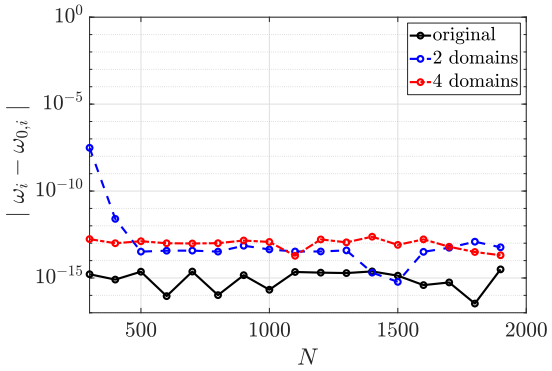

(b)

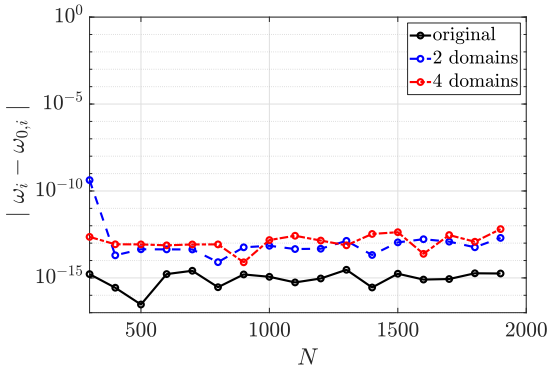

(c)

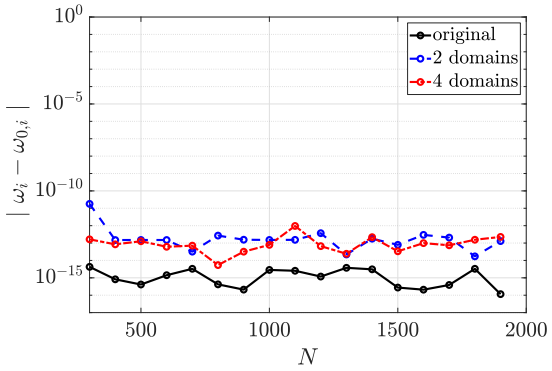

(d)

Figure 3.3: Convergence of different domain decomposition methods, $Re = 1000$. (a) $k = 0.3$, (b) $k = 1.1$, (c) $k = 1.5$, (d) $k = 2$.

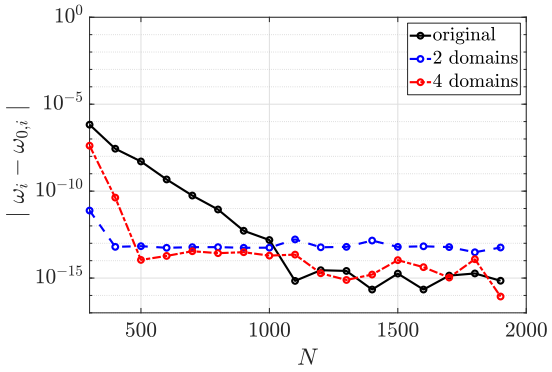

(a)

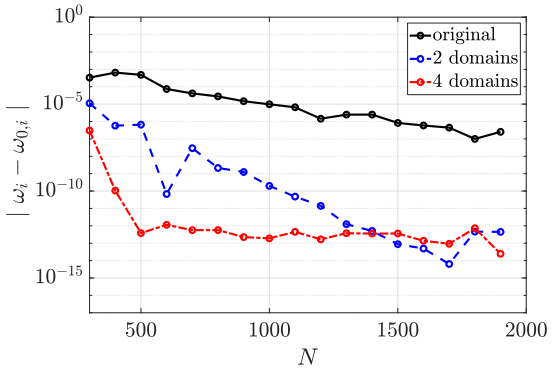

(b)

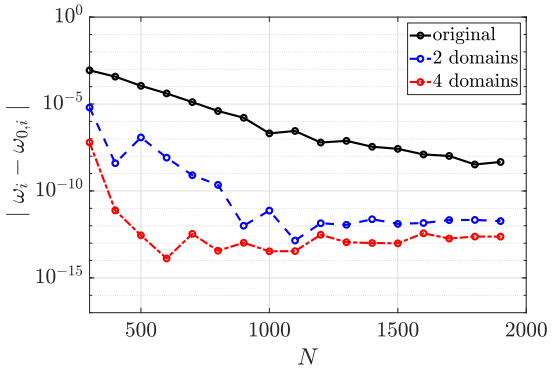

(c)

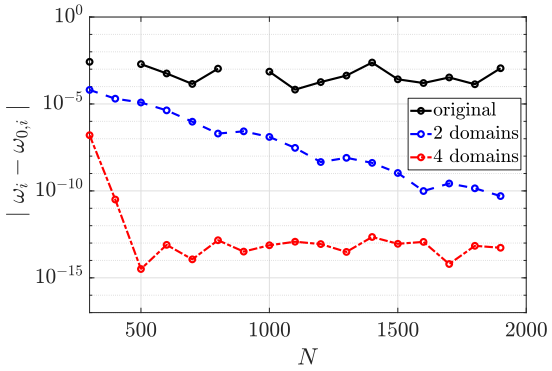

(d)

Figure 3.4: Convergence of different domain decomposition methods, $Re = \infty$, (a) $k = 0.3$, (b) $k = 1.1$, (c) $k = 1.5$, (d) $k = 3$.

Chapter 4

Results

4.1 The velocity profile

The stability of the wake downstream of a thin, symmetric, half-submerged airfoil NACA 0003 is considered. Detailed velocity measurements at various downstream locations of the wake are given by Mattingly & Criminale (1970) [2]. A hyperbolic function is used to fit the measured velocity profiles,

$$\frac{U - U_\infty}{U_c - U_\infty} = \frac{1}{\cosh^2(\sigma z/b)}, \tag{4.1}$$

where b id the half-width of the wake, and U_c is the center-line velocity. The constant $\sigma = 0.88137$ is chosen so that $(U - U_\infty)/(U_c - U_\infty) = 0.5$ at $z = b$, as given in Dimas (1988) [1].

Local stability for near-wake is considered, and the velocity profile used throughout this thesis is the velocity profile fitted at a location downstream of the airfoil $x/L = 0.003$, where L is the chord length of the airfoil. The corresponding center-line velocity is $U_c/U_\infty = 0.0012$.

Bibliography

[1] A. A. Dimas. *Interaction between a two-dimensional wake and the free surface at low Froude numbers*. Thesis, 1988.

[2] G. E. Mattingly and W. O. Criminale. The stability of an incompressible two-dimensional wake. *Journal of Fluid Mechanics*, 51(2):233–272, 1972.

[3] C. B. Moler and G. W. Stewart. Algorithm for generalized matrix eigenvalue problems. *Siam Journal on Numerical Analysis*, 10(2):241–256, 1973.

[4] P. Schmid and D. Henningson. *Stability and Transition in Shear Flows*, volume 142. 2001.

A. Stress balance at the free surface